Published in final edited form as:
Nat Immunol. 2017 October ; 18(10): 1150–1159. doi:10.1038/ni.3813.

Caveolin-1-dependent BCR nanoscale organization regulates B cell tolerance

Susana Minguet[1,2,3,4], **Kathrin Kläsener**[1,2,5], **Anna-Maria Schaffer**[1,3], **Gina J. Fiala**[1,2], **Teresa Osteso-Ibánez**[6], **Katrin Raute**[1,2,7], **Inmaculada Navarro-Lérida**[6], **Frederike A. Hartl**[1,2], **Maximilian Seidl**[3,8], **Michael Reth**[1,2,5], and **Miguel A. Del Pozo**[6]

[1]Department of Immunology, Institute for Biology III, Faculty of Biology, University of Freiburg, Germany

[2]Centre for Biological Signalling Studies BIOSS, University of Freiburg, Germany

[3]Center for Chronic Immunodeficiency (CCI), Medical Center – University of Freiburg, Faculty of Medicine, University of Freiburg, Germany

[4]S.M. was a Ramón y Cajal fellow at the Mechanoadaptation & Caveolae Biology Lab, Cell Biology & Physiology Program; Cell & Developmental Biology Area, Centro Nacional de Investigaciones Cardiovasculares Carlos III (CNIC), Madrid, Spain from 2008 till 2011

[5]Max Planck Institute of Immunology and Epigenetics, Freiburg, Germany

[6]Mechanoadaptation & Caveolae Biology Lab, Cell Biology & Physiology Program; Cell & Developmental Biology Area, Centro Nacional de Investigaciones Cardiovasculares Carlos III (CNIC), Madrid, Spain

[7]Spemann Graduate School for Biology and Medicine (SGBM), University of Freiburg, Germany

[8]Institute for Surgical Pathology, University Medical Center Freiburg, University of Freiburg, Germany

Abstract

Caveolin-1 (Cav1) regulates plasma membrane nano-organization and compartmentalization. Here, we demonstrate that Cav1 controlled the distribution of immunoglobulin M (IgM)- and IgD-B cell antigen receptor (BCR) nanoclusters on the surface of B cells. In mature B cells, the IgM-BCR gained access to GM1-enriched lipid domains upon antigen stimulation by a process that was dependent on Cav1 phosphorylation by Src family kinases, thereby regulating BCR signaling *in vivo*. In *Cav1*$^{-/-}$ immature B cells, altered IgM-BCR nanoscale organization resulted in a failure of receptor editing, and a skewed repertoire of B cells expressing μ heavy chains (HCs) with

Correspondence should be addressed to S.M. (susana.minguet@biologie.uni-freiburg.de).

Author contributions

S.M. designed this study, performed experiments, and wrote the manuscript with input from all authors. K.K. and A.M.S. performed the PLA experiments. G.J.F. and F.A.H. performed *ex vivo* stimulations. T.O.I. raised the mice and performed experiments. I.N.-L. performed the DRMs experiments. M.S and K.R. performed kidney analysis. M.R. gave intellectual input and conceptual and scientific advice. M.A.d.P. provided his Cav1 expertise to the conception of the project, and gave intellectual input and conceptual and scientific advice. All authors critically read the manuscript.

Competing financial interests Statement

The authors declare no conflict of interest.

Europe PMC Funders Author Manuscripts

hallmarks of poly- and auto-reactivity, which ultimately led to autoimmunity in mice. Thus, Cav1 emerges as a cell-intrinsic regulator that prevents B cell-induced autoimmunity by means of its role in plasma membrane organization.

Introduction

The B cell antigen receptor (BCR) is a multiprotein complex expressed on the surface of B cells transmitting critical signals for B cell development, proliferation and activation. The BCR consists of two identical immunoglobulin (Ig) heavy chains (HCs) and two identical light chains (LCs) forming the antigen-binding molecule, which is associated to the signal transduction unit composed of the Igα-Igβ (CD79a-CD79b) heterodimer1. Signaling from the BCR is triggered by ligand engagement and leads to B cell activation. The BCR lacks intrinsic tyrosine kinase activity but signaling is achieved by phosphorylation of its immunoreceptor tyrosine-based activation motifs (ITAMs)2 by Src family protein tyrosine kinases such as Lyn and the spleen tyrosine kinase (Syk)3. Syk recruitment to phosphorylated ITAMs amplifies BCR signal transduction4.

BCR signaling ensures the generation of a naïve antibody repertoire, from which autoreactive specificities have been removed5. During early B cell development in the bone marrow (BM), the variable Ig gene segments are stochastically recombined generating an enormous (10^{11}) diversity of antibody specificities6,7. This process can generate BCRs that recognize the body's self-components and potentially leads to autoimmunity. To silence these autoreactive BCRs, central tolerance is established by mechanisms such as deletion, anergy and receptor editing8,9. It has been estimated that 25–50% of the naturally arising antibodies in mice undergo receptor editing by LC replacement10,11. In humans, up to 75% of the newly generated antibodies are potentially self-reactive but are efficiently removed during B cell development12. Decreased BCR signaling impairs the counter-selection of autoreactive B cells by failing to induce tolerance mechanisms at immature B cells in mice and humans13–15.

Immature B cells exclusively express IgM-BCRs, whereas mature B cells co-express both IgM- and IgD-BCRs of identical antigen-specificity. Both receptors form nanoclusters on the surface of resting B cells (also named protein islands)16–20. The IgM- and IgD-BCRs reside in different class-specific membrane compartments with distinct protein and lipid compositions18–20. The IgD-compartment is enriched in ordered lipid domains, while the IgM-BCR gains access to these lipids only after B cell activation. Recent reports suggest that BCR nanoclustering is important for shaping BCR signaling18,20. To date, little is known about how such a membrane organization is regulated at the molecular level.

Caveolin-1 (Cav1) is a membrane protein that promotes the assembly and stability of ordered lipid domains in several cell types21. In addition, Cav1 modulates the assembly and activity of multimolecular signaling complexes through interactions with its phosphorylated Tyr14 or its scaffolding domain21,22. Increased lipid mobility, enhanced abundance of ordered domains and accelerated endocytosis have been reported in cells lacking Cav1 expression23–25. It was initially reported that lymphocytes do not express Cav1 based on the analysis of several B and T cell lines26. However, more recent studies proved a role for

Europe PMC Funders Author Manuscripts

Cav1 in primary T cells27,28. Furthermore, Cav1 has been detected in splenic B cells upon lipopolysaccharide (LPS) stimulation, and appears to play a role in T-independent (TI) antibody responses *in vivo*29.

Given the role of Cav1 in membrane compartmentalization, we hypothesized that Cav1 regulates the IgM- and IgD-BCRs nanoscale distribution on the surface of B cells. Our results clearly show that the IgM-BCR gained access to GM1-enriched domains upon BCR triggering by a process that was regulated by the phosphorylation of Cav1 by Src family kinases. Accordingly, *Cav1*$^{-/-}$ mature B cell activation *in vivo* and *ex vivo* was impaired and *Cav1*$^{-/-}$ immature B cells showed reduced receptor editing resulting in a skewed BCR repertoire of μHC with hallmarks of poly- and auto-reactivity. Correspondingly, *Cav1*$^{-/-}$ mice exhibited splenomegaly, high titers of serum autoantibodies, spontaneous germinal centers (GC) and a reduced life span.

Results

Cav1 regulates nanoclustering of the IgM-BCRs

Primary B cells expressed Cav1 (Supplementary Fig. 1a). Therefore, we investigated whether Cav1 regulates the nanoscale organization of the IgM- and the IgD-BCR on the surface of B cells. We performed *in situ* proximity-ligation assay (PLA) using non-permeabilized primary B cells from wild-type and B6.CavKO30 mice to quantify the proximity between the BCR and the cholera toxin B subunit (CTxB) on the B cell surface (Supplementary Fig. 1b). CTxB binds with high affinity to GM1 glycolipids, which are highly expressed in cholesterol- and sphingolipid-rich membrane domains, also known as ordered lipid domains31. Controls were performed in resting and pervanadate (perV) stimulated primary B cells (Supplementary Fig. 1c). As reported18, in resting wild-type splenic B cells, the IgM-BCR was mainly excluded from GM1-enriched domains (Fig. 1a). However, in *Cav1*$^{-/-}$ resting B cells, a significant proportion of IgM-BCRs was found in close proximity to GM1 (Fig. 1a). On the surface of wild-type B cells, the IgM-BCR proximity to GM1-lipids reached a maximum at five minutes upon BCR-triggering and decreased to basal levels after 20 minutes, likely due to BCR internalization (Supplementary Fig. 1d). On *Cav1*$^{-/-}$ B cells, the already high IgM-BCR-GM1 proximity remained unchanged upon stimulation either with anti-BCR or perV (Fig. 1a). Cav1 was next expressed in the Cav1-deficient murine B cell line K46 in a gain-of-function approach (Supplementary Fig. 1e,f). Again, the IgM-BCR gained access to GM1-enriched lipid domains upon B cell activation only in K46 cells expressing Cav1 as seen by PLA (Supplementary Fig. 1e) or by purification of detergent-resistant membranes (DRMs, Supplementary Fig. 1f). Lack of Cav1 did not globally disrupt membrane topology since basal amounts of DRM-associated molecules, such as GM1 and LYN, were similar between cells expressing either Cav1, a non-phosphorylatable Cav1 mutant or lacking Cav1 expression. BCR-induced Rac1 translocation to DRMs, which is required for its activation, only occurred in the presence of Cav1 (Supplementary Fig. 1f), suggesting defective BCR-induced signaling in *Cav1*$^{-/-}$ B cells. Taken together, Cav1 regulates the nanoscale distribution of the IgM-BCR both in the resting state and upon BCR stimulation.

Phosphorylation of Cav1 regulates BCR nanoclustering

We next investigated the role of Src family kinases in the reorganization of IgM-BCRs upon BCR activation by incubating primary B cells with the Src kinase inhibitor PP2. Translocation of the IgM-BCR to GM1-enriched lipid domains in *Cav1*$^{+/+}$ B cells was significantly blocked in the presence of PP2 comparable to that seen in *Cav1*$^{-/-}$ B cells (Fig. 1b). Src family kinases have been reported to phosphorylate both the BCR32 and Cav1 at Tyr14 (ref. 33). To clarify whether Cav1 phosphorylation regulates IgM-BCR membrane compartmentalization, we purified B cells from mice carrying a non-phosphorylatable Cav1 mutant (B6.*Cav1*$^{Y14F/Y14F}$)28. Both the steady-state and the activation-induced distribution of the IgM-BCR in relation to GM1-enriched lipid domains were modulated by Cav1 Tyr14 phosphorylation (Fig. 1c). IgM- and IgD-BCRs are found in separated class-specific compartments in wild-type B cells that only coalesce upon B cell stimulation34. In comparison to resting wild-type splenic B cells, the proportion of IgD-BCRs close to GM1-enriched lipid domains was significantly reduced in *Cav1*$^{-/-}$ resting B cells (Fig. 1d). BCR stimulation reduced IgD-BCR proximity to GM1-enriched lipid domains in wild-type B cells but not in *Cav1*$^{-/-}$ nor in *Cav1*$^{Y14F/Y14F}$ B cells, indicating that the activation-induced distribution of IgD-BCRs is regulated by Cav1 Tyr14 phosphorylation (Fig. 1d). The steady-state BCR class-specific separation was disturbed both in *Cav1*$^{-/-}$ and *Cav1*$^{Y14F/Y14F}$ B cells (Fig. 1e). Upon BCR stimulation, the coalescence of IgM- and IgD-BCRs was reduced in *Cav1*$^{Y14F/Y14F}$ B cells and abolished in *Cav1*$^{-/-}$ B cells (Fig. 1e). Importantly, the steady-state IgM- and IgD-BCR surface expression and the BCR internalization kinetics were indistinguishable in *Cav1*$^{+/+}$, *Cav1*$^{-/-}$ and *Cav1*$^{Y14F/Y14F}$ B cells (Supplementary Fig. 2a,b). Thus, Cav1 phosphorylation at Tyr14 is required for the steady-state separation between IgM- and IgD-BCRs and for the optimal reorganization of both BCR isotypes upon stimulation.

The BCR gains proximity to Cav1 upon B cell activation

Next, we investigated whether the cytoplasmic part of the BCR, namely Igα, also gains proximity to Cav1 upon BCR triggering by *in situ* PLA in permeabilized cells (Supplementary Fig. 2c,d). In resting primary B cells, the cytoplasmic part of the BCR and Cav1 are >40 nm apart as no PLA signal was detected (Fig. 2). Upon B cell activation, the BCR and Cav1 gained proximity to each other gradually for the first 15 minutes upon stimulation (Fig. 2). This proximity was induced by anti-IgM or perV treatment but was independent of Cav1 Tyr14 phosphorylation (Fig. 2). Similar results were obtained with K46 cells expressing Cav1 (Supplementary Fig. 2e). Taken together, B cell activation is accompanied by increase proximity between the cytoplasmic regions of the BCR and Cav1, and this reorganization does not require Tyr14 phosphorylation. These results are compatible with a lateral reorganization of the BCR within the plasma membrane and with conformational changes in the Igα cytoplasmic tail35.

Reduced B cell activation in mice lacking Cav1

Our results show that in the absence of Cav1, the nanodistribution of the IgM- and the IgD-BCRs is altered. To investigate the implications for B cell activation *in vivo*, we used two Cav1-deficient models that differ in the disrupted exon and their genetic background: exon 3

in a C57BL/6 background (B6.CavKO30) and exon 2 in a mixed background (129/Sv, C57BL/6J and SJL, hereafter referred to as CavKO36). B6.Cav1KO and Cav1KO mice were immunized with alum-precipitated TI antigen nitrophenol (NP)-Ficoll. The proportion of antigen-specific B cells was significantly reduced in the spleens of both Cav1-deficient models compared to wild-type controls (Fig. 3a,b and Supplementary Fig. 3a,b). Further, clonal expansion of splenic B cells as measured by Ki-67 staining was also decreased (Fig. 3c and Supplementary Fig. 3c). NP-specific antibody-secreting cells and NP-specific serum antibodies were significantly reduced (Fig. 3d,e). In agreement with the previous report29, no differences were observed upon TD responses (data not shown).

To address whether impaired BCR-induced signaling was responsible for the reduced *in vivo* responses, we performed *ex vivo* stimulation of splenic B cells. First, BCR-induced proliferation was reduced in both Cav1-deficient models whereas stimulation with LPS resulted in equivalent strong proliferation as compared to wild-type controls, indicating that signaling from the BCR was specifically affected (Fig. 3f and Supplementary Fig. 3d). Second, B cells from both Cav1-deficient models showed a reduction in BCR-induced expression of the early activation markers CD69 and CD86 (Fig. 3g,h and Supplementary Fig. 3e). Third, reduced calcium flux responses upon BCR-triggering were monitored in primary cells lacking Cav1 from both animal models (Fig. 3i and Supplementary Fig. 3f). Last, phosphorylation of Syk, which is crucial for signal transduction from the BCR, was decreased in *Cav1*$^{-/-}$ B cells compared to wild-type cells (Fig. 3j). *Cav1*$^{Y14F/Y14F}$ B cells exhibited a milder phenotype regarding BCR-induced signaling (Fig. 3g,h,j). Hence, B cell activation is reduced both *in vivo* and *ex vivo* in the absence of Cav1 expression as shown by two independent Cav1-deficient mice models.

Aged *Cav1*$^{-/-}$ mice develop features of autoimmunity

CavKO mice have a reduced life span that was previously attributed to secondary complications such as pulmonary fibrosis, hypertension or cardiac hypertrophy37. We confirmed those data (Supplementary Fig. 4a) and extended the findings to the B6.CavKO model (Fig. 4a). Mutant mice in both models exhibited large spleens, which were detectable from 15 weeks of age onwards and became more obvious in aged mice (Fig. 4b and Supplementary Fig. 4b,c). Both the total number and the proportion of B cells in the spleens were significantly increased in Cav1-deficient mice as compared to wild-type controls (Fig. 4c,d and Supplementary Fig. 4d). In aged mice, spontaneously generated GC and class-switched B cells were significantly increased (Fig. 4e,f and Supplementary Fig. 4e,f). Proliferating Ki-67^{+} B cells formed morphological structures resembling clonally expanding B cells in the spleen of aged mice (Supplementary Fig. 4g). IgG immunocomplexes were elevated in kidneys of aged Cav1-deficient mice when compared to aged-matched WT mice (Fig. 4g and Supplementary Fig. 4i,j). Aged Cav1-deficient mice had significantly increased serum titers of spontaneously generated anti-cardiolipin and anti-dsDNA IgG autoantibodies while total IgG concentrations were similar to age-matched wild-type controls (Fig. 4h and Supplementary Fig. 4h). No significant abnormalities were found in the myeloid or T cell linages (data not shown). Altogether, aged Cav1-deficient mice develop features of immune dysregulation characterized by spontaneous GC formation, increased B cell numbers in the spleen, elevated titers of serum autoantibodies and reduced life span.

B cell specific autoimmunity in Cav1$^{-/-}$ mice

Our data showed immune dysregulation in two Cav1-deficient mouse models. We next performed BM-chimeras to investigate the contribution of B cells to this phenotype. First, sublethally irradiated *Rag2*$^{-/-}\gamma C^{-/-}$ mice reconstituted with Cav1KO-BM showed a statistically significant reduced life span, proving that the reduced life span previously observed in Cav1$^{-/-}$ mice37 results from their dysregulated immune system (Supplementary Fig. 5a,b). After 25 weeks, the surviving animals were sacrificed and analyzed. The spleens of mice reconstituted with Cav1KO cells were significantly enlarged (Supplementary Fig. 5c) and the percentage of spontaneously generated GC B cells was increased (Supplementary Fig. 5d). Significantly increased titers of anti-cardiolipin and anti-dsDNA IgG were detected in animals reconstituted with Cav1KO cells (Supplementary Fig. 5e). Hence, the immune dysregulation in Cav1-deficient mice has its origin in their immune system.

We performed competitive BM-reconstitutions to corroborate these findings and to narrow down the population responsible for this phenotype. *Rag2*$^{-/-}\gamma C^{-/-}$ mice were reconstituted with B6.Cav1KO or B6.WT (expressing CD45.2) and wild-type (expressing CD45.1) BM cells at a 1:1 cell ratio. In the B6.Cav1KO/CD45.1WT chimera, 73 ± 3% of the B cells in the BM were Cav1$^{-/-}$ cells (Fig. 5a). A statistically significant accumulation of Cav1$^{-/-}$ B cells was detected from the immature B cell stage onwards (Fig. 5b). Similarly, Cav1$^{-/-}$ cells constituted 71 ± 2% of the splenic lymphocytes, whereas wild-type cells accounted for the expected 49 ± 0.6% of splenocytes in the B6.WT/CD45.1WT chimeras (Fig. 5c,d). In the peripheral lymph nodes, Cav1$^{-/-}$ B cells were also specifically expanded (Fig. 5e), whereas the proportions of different T populations conserved the 1:1 ratio in both chimeras in spleen, lymph nodes and thymus (Fig. 5f and Supplementary Fig. 5f-i). When spontaneously formed GC B cells were analyzed, up to 73 ± 6% of them lacked Cav1 expression (Fig. 5g). Moreover, those mice that were reconstituted with BM from B6.Cav1KO exhibited higher titers of serum autoantibodies (Fig. 5h).

Finally, *Rag2*$^{-/-}\gamma C^{-/-}$ mice were reconstituted with B6.*Cd79a*$^{-/-}$ (lacking B cells) and either B6.Cav1KO or B6.WT BM cells at a 1:1 cell ratio. In this experimental setup, Cav1$^{-/-}$ B cells do not compete with wild-type B cells but reconstituted along Cav1-expressing cells of the other hematopoietic lineages. The life span of mice reconstituted with Cav1$^{-/-}$ B cells was significantly reduced (Fig. 5i). The surviving mice had specifically expanded the B cell compartment in the spleen (Fig. 5j) and elevated serum anti-cardiolipin IgG autoantibodies (Fig. 5k). In these mice, the onset of the immune dysregulation was delayed, suggesting that Cav1 deficiency in other immune cells might collaborate to the observed phenotype.

Defective central tolerance in Cav1$^{-/-}$ mice

Central and peripheral B cell tolerance checkpoints ensure the removal of autoreactive B cells in the BM and periphery, respectively12. To identify whether these checkpoints are defective in B6.Cav1KO mice, immature B cells from the BM and splenic B cells were purified and their productive *Igh* allele transcripts were cloned and sequenced. In comparison to wild-type, the variable domains of B6.Cav1KO B cells carried longer CDR3 segments harboring more positively charged amino acids (Fig. 6a and Supplementary Fig.

6a). These features are hallmarks of autoreactivity12. Autoreactive IgH-chains are detected in immature Cav1$^{-/-}$ B cells from the BM supporting a defect in central tolerance. Cav1 mRNA was significantly abundant in immature B cells (Fig. 6b). B cell development B6.Cav1KO BM is unaltered with two exceptions: (i) a specific increase in mature recirculating B cells (Fig. 6c) and (ii) a reduced proportion of λLC^{+} cells (10% reduction, Supplementary Fig. 6b). The percent of transitional CD93^{+} B cells in the spleen of B6.Cav1KO was decreased and the proportion of anergic B cells increased (Supplementary Fig. 6c). Taken together, these data support a break in central tolerance, but a partially functional peripheral tolerance, explaining why Cav1$^{-/-}$ mice develop features of autoimmunity rather late in life.

In immature B cells newly generated BCRs are tested for autoreactivity by means of BCR signaling. We thus investigated whether Cav1 also regulates IgM-BCR nanoclustering in immature B cells. The proximity between IgM-BCR and GM1 membranes increased upon stimulation in wild-type immature B cells but was impaired by the expression of Cav1Y14F or the absence of Cav1 (Fig. 7a). The immature B cell line WEHI-231 (henceforth referred to as WEHI) has proven to be a useful model for the study of BCR-induced apoptosis and clonal deletion of immature B cells. WEHI barely express Cav1 as described for other lymphoid cell lines26. In a gain-of-function experiment, Cav1-IRES-GFP and IRES-GFP vectors were expressed in WEHI cells. IgM-BCR and GM1 membranes coalesced, and BCR and Cav1 gained proximity upon activation (Supplementary Fig. 7a,b). When WEHI cells were stimulated, cells expressing Cav1 (GFP^{+}) underwent a stronger apoptosis response than their GFP^{-} counterparts (Supplementary Fig. 7c). Our data suggest that by compromising IgM-BCR membrane reorganization and signaling, Cav1 deficiency impacts the efficient removal of autoreactive immature B cells.

We next established an *in vitro* system mimicking the encounter of an autoantigen by immature B cells. BM from B6.Cav1KO and B6.WT mice were cultivated under conditions in which B220^{+}IgM^{+} immature B cells were present (Supplementary Fig. 7d). Next, anti-IgM Fab'2 was added to the cultures mimicking autoantigen. The proportion of IgM-expressing cells and IgM-BCR surface expression were only reduced in wild-type cells (Supplementary Fig. 7d,e). Upon BCR activation of immature B cells, efficient receptor editing leads to an increased use of λLC38. Immature Cav1$^{-/-}$ B cells failed to increase the λLC expression upon activation *in vitro* (Fig. 7b). Next, B6.Cav1KO mice were crossed with 3-83Igi mice, which express gene-targeted *Igh* and *Igk* loci encoding an autoreactive BCR composed of 3-83Hi HC and 3-83κi LC39. The 3-83 BCR is autoreactive on the H-2^{b} background (B6). The percent of λLC^{+} B cells is the best indicator of receptor editing in this model since WT κLC pairing with 3-83Hi create a high frequency of autoreactive receptors. Three littermate groups were analyzed: mice expressing both the 3-83 HC and LC (3-83Hi:3-83κi), only the 3-83 HC (3-83Hi:WT) or only the 3-83 κLC (WT:3-83κi). The percentage of λLC^{+} cells in WT:3-83κi mice was similar to non-transgenic mice (data not shown), indicating that pairing of endogenous HC with the 3-83κi did not create autoreactive receptors (Fig. 7c,d). Pairing of the 3-83Hi with WT LC, in contrast, generated autoreactive receptors as demonstrated by a significant increase of λLC^{+} B cells (Fig. 7c,d). The highest percentage of λLC^{+} cells was observed in 3-83Hi:3-83κi mice (Fig. 7c,d). In Cav1-deficient mice expressing 3-83Hi:3-83κi and 3-83Hi:WT autoreactive BCRs, the

percentage of λLC^+ B cells was statistically reduced compared to mice expressing Cav1 (Fig. 7c,d). Altogether, our data support a model in which Cav1 regulates the nanoscale distribution of the BCR, thereby controlling BCR activation. In immature B cells, defects in this distribution result in sub-optimal receptor editing leading to a break in B cell tolerance.

Discussion

Our data demonstrate that Cav1 regulates hallmarks of IgM- and IgD-BCR nanoclustering on the surface of resting B cells: (1) efficient exclusion of the IgM-BCR from GM1-enriched lipid domains; (2) IgD-BCR close proximity to those lipids and (3) class-specific segregation of IgM- and IgD-BCRs. Thus, the previously described organization of the IgM- and IgD-BCR protein islands or nanoclusters16–18,20,34,40 requires Cav1. We have identified Cav1 as a molecular target that allows the manipulation of the nanoscale organization of B cell plasma membrane. Whether Cav1 orchestrates this basal compartmentalization during the sorting process at the Golgi or by scaffolding the IgD-BCR in GM1-enriched lipid domains, while excluding the IgM-BCR, remains to be investigated. Likewise, the motifs at the IgM- and IgD-BCR that mediate this class-specific compartmentalization must be identified. Importantly, cholesterol- and sphingolipid-rich domains exist in the absence of Cav1 in several cell types including lymphocytic cell lines26 and we showed here that the composition of these domains does not dramatically change in Cav1-deficeint B cells. Therefore, it is very unlikely that our results are just a consequence of the lack of these domains in $Cav1^{-/-}$ B cells. In the steady state, BCR nanoclustering was regulated by phosphorylation of Cav1 in Tyr14. Cav1 is phosphorylated in resting B cells41 and might recruit CSK (C-terminal SRC kinase)42 to mediate actin organization43 preventing thereby, BCR diffusion in the plasma membrane20.

BCR stimulation results in a rapid coalescence of the IgM-BCR with GM1-enriched domains44, IgD-BCR diffusing from these domains18 and coalescence of IgM and IgD nanoclusters34. Treatment of B cells with the F-actin inhibitor Latrunculin-A results in cell activation20, suggesting that relaxing the actin cytoskeleton promotes diffusion in the membrane and the coalescence of the BCR nanoclusters for signal propagation. Herein, we show that all these translocations were impaired in the absence of Cav1, suggesting a connection between the BCR, Cav1 and actin reorganization upon BCR stimulation. This connection might be mediated by the BCR-mediated recruitment of SHP2 to the membrane, which competes with CSK for binding to phosphorylated Cav142. CSK is thus released from the membrane and the actin cytoskeleton relaxed. Alternatively, localization of Ezrin-Radixin-Moesin-family of proteins to Cav1 and GM1-enriched domains45 or interaction of Filamin A with Cav1 and actin46 might mediate this connection. Ligand-induced IgM-BCR redistribution is sensitive to Src family kinase-inhibition by PP247. These data were previously interpreted as an indication that the phosphorylation of the BCR-ITAMs drives this reorganization. Herein, we demonstrated that the Tyr14 in Cav1 contributes to the translocation of the IgM-BCR into, and of the IgD-BCR out of GM1-enriched domains, opening the discussion of how ligand-induced BCR signaling and Cav1 phosphorylation regulate BCR reorganization. Our data conclusively show that in $Cav1^{-/-}$ B cells, IgM- and IgD-BCR islands fail to coalesce upon activation and that BCR signaling is impaired, but not fully abolished. In contrast, IgM- and IgD-BCR domains coalesced in $Cav1^{Y14F/Y14F}$ B

Europe PMC Funders Author Manuscripts

cells, which showed a milder reduction of B cell activation. Taken together, these data suggest that IgM- and IgD-BCR coalescence is a crucial step for efficient BCR signaling.

Despite B cell dysfunction, aged B6.Cav1KO mice developed features of autoimmunity such as spontaneous B cell activation, elevated autoantibodies titers, reduced lifespan and IgG deposits in the kidneys. These hallmarks of autoimmunity were observed in two independent Cav1-deficient mice models with different genetic backgrounds and in BM transfer experiments, enforcing their relevance. B cell-mediated autoimmunity has been associated with increased BCR signaling in the periphery or with failures in the elimination of autoreactive B cells. $Cav1^{-/-}$ peripheral B cells are not hyperactive. Therefore, Cav1 appears to be important for the efficient removal of autoreactive B cells, as supported by the skewed BCR repertoire and the presence of autoantibodies in Cav1-deficient mice. Autoreactive $Cav1^{-/-}$ B cells in the periphery might become activated by high autoantigen concentrations and co-stimulatory signals from T cells and/or Toll-like receptors, driving autoimmunity. Data in humans suggest that the threshold of BCR activation in the immature stages might define self-tolerance. For instance, alterations in Lyn expression have been reported in Lupus patients48. Further, patients who carry mutations in Btk display a high frequency of autoreactive immature B cells49. Thus, $Cav1^{-/-}$ mice emerge as a meaningful model showing that reduced BCR signaling can lead to autoreactivity and recapitulates the self-reactivity associated to defects in BCR signaling observed in common variable immunodeficiency and X-linked agammaglobulinemia patients.

The difference in the outcomes upon activation of the IgM-BCR in immature and mature B cells is not clearly understood. Using WEHI as an immature B cell model, it was reported that the IgM-BCR failed to translocate to GM1-enriched domains upon activation, proposing that BCR signal initiation outside of these platforms in immature B cells activates a different cell-fate program, namely receptor editing or apoptosis50. However, we did not detect Cav1 expression in WEHI cells. Upon Cav1 re-expression, however, the IgM-BCR efficiently reorganized to GM1-enriched domains enhancing IgM-induced apoptosis. Likewise, $Cav1^{-/-}$ immature B cells failed to reorganize the IgM-BCR upon stimulation and to initiate receptor editing by exchanging their LC. Therefore, both in immature and mature B cells, ligand-induced BCR reorganization is necessary for efficient signaling.

In summary, we have identified Cav1 as a regulator of the nanoscale organization of the IgM- and the IgD-BCR in the plasma membrane of B cells. By targeting Cav1, we have demonstrated that BCR nanoclustering is crucial to set the threshold of activation of both mature and immature B cells. In immature B cells, the absence of Cav1 results in deficient counterselection of B cells expressing autoreactive BCRs, which ultimately leads to autoimmunity in mice. This work underlines the emerging concept that immunodeficiencies often manifest as autoimmunity and will boost our knowledge of immune dysregulatory diseases.

Online Methods

Cells and mice

The murine B cell line K46 and its nitrophenol (NP)-specific mIgD- and mIgM-BCR expressing transfectant K46μmL was previously described51. K46μmL and WEHI-231 cells were cultured in RPMI-1640 complete medium supplemented with 10% fetal calf serum (FCS), 2 mM L-glutamine, 100 U/ml penicillin/streptomycin and 50 μM 2-mercaptoethanol and grown at 37 °C in a humidified atmosphere with 5% CO_2. The B6.Cav1KO30, Cav1KO36, 3-83Igi39 B6.*Cav1*$^{Y14F/Y14F}$ (ref. 28), B6.*Cd79a*$^{-/-}$52, *Rag2*$^{-/-}$ γc$^{-/-}$ and B6.CD45.1 (C57BL/6-Ly5.1) mice were bred under specific pathogen-free conditions. Mice were sex-matched and age-matched with littermate controls whenever possible. All animal protocols (G12/64) were performed according to the German animal protection law with permission from the responsible local authorities.

Flow cytometry

Organs were collected, processed to single-cell suspension, and erythrocytes removed by incubation in erythrocyte lysis buffer 150 mM NH_4Cl and 10 mM $KHCO_3$ for 4 min at about 20 °C. 0.3–0.5 × 10^6 cells were stained on ice and in the dark for 20 min in PBS containing 1% FCS and the indicated antibodies. Before analysis, cells were washed a minimum of two times. Measurements were performed using a CyanTM (Beckham Coulter) or LSR II (BD Biosciences) Flow Cytometer and analyzed with the FlowJo software.

Antibodies

The following antibodies were used for immunoblotting: anti-SYK (N-19; Santa Cruz), anti-IgM-HRP (Southern Biotech), anti-Cav1 (D46G3; Cell Signaling), anti-RAC1 (Millipore), anti-LYN (Cell signaling) and anti-Tubulin (Sigma).

The following antibodies were used for flow cytometry: anti-B220-PECy7 (RA3-6B2), anti-IgD (11-26), anti-IgM (polyclonal), anti-CD19 (1D3), anti-CD4 (GK1.5 and RM4-5), anti-CD8 (53-6.7), anti-CD93 (AA4.1), anti-CD69-PECy7 (H1.2F3), anti-CD86-PE (GL-1), anti-GL7, anti-CD95 (15A7) (all from eBioscience), anti-λLC λ1, λ2 & λ3 (R26-46), anti-κLC (187.1), anti-CD45.1 (A20), anti-IgD-FITC (11-26c.2a), anti-CD45.2 (105), Ki-67 (B56) (all from BD Pharmingen), anti-CD19 (6D5) (Biolegend). NP-BSA-biotin was from Biosearch Technologies. Anti-IgM-Fab'2-Alexa 649 was from Jackson ImmunoResearch (goat polyclonal). CSFE was from Sigma.

B cell purification and *in situ* Proximity-Ligation Assay (PLA)

For PLA, the following reagents were used: anti mouse-Cav1 (Cell Signaling), anti-mouse-Igα(HM47/A9 - BSA and Azide free, Abcam), anti-mouse-IgM, (clone 1B4B1, Southern Biotech), anti-mouse-IgD (clone 11-26c.2a, Southern Biotech) and CTxB (Sigma-Aldrich). Fab fragments were prepared of anti-IgM, anti-IgD and anti-Igα with Pierce Fab Micro preparation kit (Thermo Scientific) using immobilized papain according to the manufacturer's protocol. After desalting (Zeba spin desalting columns, Thermo Scientific), the Fab fragments and CTxB were coupled with PLA Probemaker Plus or Minus oligonucleotides (Sigma-Aldrich) to generate PLA probes. Binding of anti-Cav1 antibody

was detected with oligo-coupled secondary anti rabbit antibodies (Sigma-Aldrich). Untouched B cells were purified from spleen using the MACS B cell isolation kit (Miltenyi Biotech). Purity was >90% as confirmed by flow cytometry using anti-CD19. The PLA between the BCR and CTxB in non-permeabilized cells was previously described18. In brief, B cells were settled onto polytetrafluoroethylene slides (Thermo Fisher Scientific) for 30 min at 37 °C. BCR stimulation was performed with 5 μg/ml goat anti-mouse IgM Fab′2 (Southern Biotech), anti-mouse IgD Fab′2 (Southern Biotech) or 0.5 mM of pervandate as indicated in each figure. Pervanadate was freshly prepared for each experiment with equal molar amounts of orthovanadate and H_2O_2. For Src-kinase inhibition, cells were pre-treated with 10 μM PP2 (Sigma-Aldrich) for 60 min before the stimulation. Upon stimulation, cells were fixed with 4% PFA at about 20 °C for 20 min. For intracellular PLA, cells were permeabilized after fixation with 0.5% saponin (Sigma-Aldrich, S7900) in PBS for 30 min. After blocking for 30 min, the cells were incubated with appropriate PLA probes in PBS. PLA reactions were conducted according to the manufacturer's protocol. Resulting samples were directly mounted on slides with DAPI Fluoromount-G (SouthernBiotech) to visualize the PLA signals in relationship to the nuclei. To perform a PLA between Cav1 and the BCR, cells were first fixed, then permeabilized and the PLA performed between oligo-labeled anti-Igα-Fab (HM57; ThermoScientific) fragments and an oligo-labeled secondary antibody recognizing an anti-Cav1 antibody (D46G3; Cell Signaling). Microscope images were acquired with a Zeiss 780 Meta confocal microscope (Carl Zeiss). For each experiment a minimum of 300 splenic cells or 100 immature cells was analyzed using the BlobFinder software and validated using ImageJ. Blob size was defined as pixel size of 5x5. Raw data were exported to Prism software (GraphPad Software). For each sample, the mean PLA signal count per cell was calculated from the corresponding images. In all PLA experiments, the data were normalized to the pervanadate stimulation in order to pool independently performed experiments since the number of dot per cell varies between experiments. The PLA between IgM- and IgD-BCR was performed as previously described34.

Cell stimulation and protein purifications

Purified B cells were starved for 1 h and then stimulated for the indicated times at 37 °C with 10 μg/ml anti-mouse IgM Fab'2 (Dianova) antibody or with 0.5 mM pervanadate for 3 min. Treatment with the SRC family kinase inhibitor PP2 (Sigma) was performed at a concentration of 20 μM for 30 min at 37°C prior to stimulation. RIPA buffer was used for cell lysis. Phospho-tyrosine immunoprecipitations were done with 4G10-sepharose (Sigma). Lipid-ordered detergent-resistant membranes (DRMs) were prepared as previously described53.

Ex vivo stimulations and Ca^{2+}-flux

For *ex vivo* stimulations, purified splenic B cells (0.2×10^6 /sample) were kept in RPMI containing 10% FCS, 2 mM L-glutamine, 100 U/ml penicillin/streptomycin, and 50 μM 2-mercaptoethanol at 37 °C in a humidified atmosphere with 5% CO_2, and incubated with the indicated stimuli for 18 h before stained with anti-CD19-PB (6D5) (BioLegend) and anti-CD69-PECy7 (H1.2F3), anti-IgM and anti-CD86-PE (GL-1) (eBioscience).

For proliferation experiments, purified B cells (0.2×10^6/sample) were labeled with CFSE in PBS containing 0.5% bovine serum albumin (BSA) according to manufacturer's instructions (Invitrogen) for 10 min at 37 °C in the dark and 5 min on ice. After three days in culture with the indicated stimuli (3 μg/ml anti-IgM Fab'2 fragments (Dianova) or 1 μg/ml LPS (Sigma)) in the presence of 0.5 ng/ml IL-4 (Peprotech). Cells were stained with PB-labeled anti-CD19 (6D5) (Biolegend) and CFSE fluorescence of the $CD19^+$ cells was measured by flow cytometry.

For Ca^{2+}-flux analysis, B cells were labeled with 5 μg/ml Indo-1 and 0.5 μg/ml pluronic F-127 (both from Molecular Probes, Life Technologies) for 45 min in RPMI containing 1% FCS in the dark. Cells were washed and kept on ice until measurement. The baseline was recorded and cells stimulated with the indicated antibody. The change in Ca^{2+}-bound / Ca^{2+}-unbound Indo-1 ratio was recorded with a LSRII fluorescence spectrometer (BD Biosciences). Data were analyzed with the FlowJo software.

BM cultures and BM chimeras

BM cultures were prepared from freshly isolated BM cells following erythrocyte lysis. Cells were cultured in IMDM containing 10% FCS, 100 U/ml penicillin/streptomycin, 50 μM 2-mercaptoethanol and interleukin 7 (IL-7) at 37 °C with 7.5% CO_2 for 2 days. Then one half of the culture supernatant was removed and substituted by the same medium without IL-7. Survival and surface protein expression was analyzed by flow cytometry.

For BM chimeras, untouched hematopoietic stem cells were purified using the MACS cell linage depletion kit (Miltenyi Biotech) from freshly isolated BM cells following erythrocyte lysis. Equal numbers of cells were injected into sub-lethally (400 rad) irradiated *Rag2*$^{-/-}\gamma c^{-/-}$ mice. After the indicated time, the animals were killed and analyzed for reconstitution.

Immunizations

To immunize mice, 4-hydroxy-3-nitrophenol conjugated to AECM-Ficoll (NP-Ficoll, Biosearch Technologies) was alum-precipitated by mixing (1 mg/ml) with an aluminum hydroxide solution at a 1:1 ratio. Precipitation in Alum makes hapten-Ficoll a modestly stronger antigen54. Mice were immunized i.p. with 376 μg per 100 gram body weight. After 7 days, mice were killed and single-cell suspension of the spleen was analyzed by flow cytometry and ELISPOT assay performed as previously described55. For presence anti-NP antibodies, mice we immunized as afore-described and blood collected every 7 days.

ELISA, repertoire analysis and quantitative RT-PCR

Quantification of total IgG antibodies and IgG autoantibodies recognizing dsDNA and cardiolipin was performed by ELISA as previously described56 with minor modifications. In detail, eight serial dilutions were done and the half maximal effective concentration (EC_{50}) calculated for each mouse. The same approach was taken for the analysis of anti-NP antibodies after immunization. For repertoire analysis, total RNA was extracted from sorted populations of B6.WT or B6.CavKO mice. cDNA was prepared and *Igh* rearrangements were amplified by RT-PCR as described56. For qRT-PCR, total RNA of sorted populations

was extracted and converted into cDNA. Mouse *Cav1* mRNA was quantified with SYBR green assay (Applied Biosystems). *Gapdh* amplifications were used as normalization controls. The following primers were used:

Cav1 (forward) 5′-CAAGCATCTCAACGACGACG-3′,

Cav1 (reversed) 5′-GCAATCACATCTTCAAAGTCAATCTT-3′,

Gapdh (forward) 5′-TGAAGCAGGCATCTGAGGG-3′ and

Gapdh (reverse) 5′-CGAAGGTGGAAGAGTGGGAG-3′.

Kidney analysis

1.5-μm sections were cut from formalin-fixed paraffin embedded kidneys and placed on coated objective plates. Deparaffination was performed in xylol followed by ethanol with increasing aqueous fractions. Heat-mediated epitope retrieval was performed in a steamer with Tris-HCl pH 6.1 for 20 min. After avidin-biotin blocking (Dako) and blocking with 5% mouse serum (Jackson Immunoresearch), slides were incubated with the biotinylated anti-mouse antibody of the K5005 kit and stained with an alkaline-based red chromogen reaction from the same kit (Dako) according to the manufacturers' guidelines. Afterwards, counterstaining was performed with hematoxylin and methenamine silver stain to highlight basement membranes and effectively distinguish proteins that are pathologically deposited from proteins in the plasma. A protocol of blind assessment and analysis by a trained pathologist was applied.

Statistical analysis

GraphPad Prism was used for data analysis and arrangement. For comparison of two data sets, two-tailed Student's *t* test was used. For comparison of three or more data sets, one-way ANOVA followed by Dunnett's multiple comparisons post-test were performed. Details on sample size, experimental replicates and statistics are included in the figure legends.

Data availability statement

The data that support the findings of this study are available from the corresponding author upon reasonable request.

Supplementary Material

Refer to Web version on PubMed Central for supplementary material.

Acknowledgements

This work was supported by the German Research Foundation (DFG) through the SFB1160 IMPATH P5 to S.M. supporting F.A.H. and A.M.S., MI1942/2-1 to S.M. supporting G.J.F., Excellence Initiative GSC-4 (Spemann Graduate School) to K.R., and EXC294 (BIOSS) to S.M. and M.R.. M.R. received support from grants TRR130-P02, SFB746-P07 and ERC-grant 32297. M.A.d.P. received support from grants SAF2008-02100, SAF2011-25047, CSD2009-00016 and SAF2014-51876-R from MINECO (Spanish Ministry of Economy and Competitiveness) and 15-0404 from the Worldwide Cancer Research Foundation. S.M. was initially supported by SAF2008-02100 (2008) and the Ramón y Cajal Program from the MINECO (2009-2011). I.N.-L. was supported by the Asociación Española Contra el Cáncer (AECC). The CNIC is supported by the Spanish Ministry of Economy and

Competitiveness (MINECO) and the Pro-CNIC Foundation, and is a Severo Ochoa Center of Excellence (SEV-2015-0505). We appreciate the BIOSS toolbox for providing us with reagents. We thank M.C. Guadamillas and A. Cerezo for the generation of the B6.*Cav1*$^{Y14F/Y14F}$ mice and M.A.d.P. for providing them. We thank E. Hobeika for sharing the *Cd79a*$^{-/-}$ mice and H. Jumaa for sharing the 3-83Igi mice. We thank C. Johner, U. Stauffer, N. Joswig, and K. Fehrenbach for experimental help. We thank Y. Kulathu, M. Swamy M. Rizzi, K. Schachtrup and Y.R. Carrasco for critical reading of the manuscript. We thank W. Schamel for intellectual input and scientific discussions.

References

1. Hombach J, Tsubata T, Leclercq L, Stappert H, Reth M. Molecular components of the B-cell antigen receptor complex of the IgM class. Nature. 1990; 343:760–762. [PubMed: 2304550]
2. Reth M. Antigen receptor tail clue. Nature. 1989; 338:383–384. [PubMed: 2927501]
3. Kurosaki T. Genetic analysis of B cell antigen receptor signaling. Annu Rev Immunol. 1999; 17:555–592. [PubMed: 10358768]
4. Rolli V, et al. Amplification of B cell antigen receptor signaling by a Syk/ITAM positive feedback loop. Mol Cell. 2002; 10:1057–1069. [PubMed: 12453414]
5. Meffre E, Casellas R, Nussenzweig MC. Antibody regulation of B cell development. Nat Immunol. 2000; 1:379–385. [PubMed: 11062496]
6. Tonegawa S. Somatic generation of antibody diversity. Nature. 1983; 302:575–581. [PubMed: 6300689]
7. Bassing CH, Swat W, Alt FW. The mechanism and regulation of chromosomal V(D)J recombination. Cell. 2002; 109(Suppl):S45–55. [PubMed: 11983152]
8. Gu H, Tarlinton D, Müller W, Rajewsky K, Förster I. Most peripheral B cells in mice are ligand selected. J Exp Med. 1991; 173:1357–1371. [PubMed: 1903427]
9. Shlomchik MJ. Sites and Stages of Autoreactive B Cell Activation and Regulation. Immunity. 2008; 28:18–28. [PubMed: 18199415]
10. Retter MW, Nemazee D. Receptor editing occurs frequently during normal B cell development. J Exp Med. 1998; 188:1231–1238. [PubMed: 9763602]
11. Casellas R, et al. Contribution of receptor editing to the antibody repertoire. Science. 2001; 291:1541–1544. [PubMed: 11222858]
12. Wardemann H. Predominant Autoantibody Production by Early Human B Cell Precursors. Science. 2003; 301:1374–1377. [PubMed: 12920303]
13. Menard L, et al. The PTPN22 allele encoding an R620W variant interferes with the removal of developing autoreactive B cells in humans. J Clin Invest. 2011; 121:3635–3644. [PubMed: 21804190]
14. Ng YS. Bruton's Tyrosine Kinase Is Essential for Human B Cell Tolerance. J Exp Med. 2004; 200:927–934. [PubMed: 15466623]
15. Grimaldi CM, Hicks R, Diamond B. B cell selection and susceptibility to autoimmunity. J Immunol. 2005; 174:1775–1781. [PubMed: 15699102]
16. Schamel WWA, Reth M. Monomeric and Oligomeric Complexes of the B Cell Antigen Receptor. Immunity. 2000; 13:5–14. [PubMed: 10933390]
17. Yang J, Reth M. Oligomeric organization of the B-cell antigen receptor on resting cells. Nature. 2010; 467:465–469. [PubMed: 20818374]
18. Kläsener K, Maity PC, Hobeika E, Yang J, Reth M. B cell activation involves nanoscale receptor reorganizations and inside-out signaling by Syk. eLife. 2014; 3:1497–17.
19. Maity PC, Yang J, Klaesener K, Reth M. The nanoscale organization of the B lymphocyte membrane. BBA - Mol Cell Res. 2015; 1853:830–840.
20. Mattila PK, et al. The Actin and Tetraspanin Networks Organize Receptor Nanoclusters to Regulate B Cell Receptor-Mediated Signaling. Immunity. 2013; 38:461–474. [PubMed: 23499492]
21. Parton RG, Del Pozo MA. Caveolae as plasma membrane sensors, protectors and organizers. Nat Rev Mol Cell Biol. 2013; 14:98–112. [PubMed: 23340574]

22. Goetz JG, et al. Biomechanical Remodeling of the Microenvironment by Stromal Caveolin-1 Favors Tumor Invasion and Metastasis. Cell. 2011; 146:148–163. [PubMed: 21729786]
23. Gaus K, Le Lay S, Balasubramanian N, Schwartz MA. Integrin-mediated adhesion regulates membrane order. J Cell Biol. 2006; 174:725–734. [PubMed: 16943184]
24. Hernández-Deviez DJ, et al. Caveolin regulates endocytosis of the muscle repair protein, dysferlin. J Biol Chem. 2008; 283:6476–6488. [PubMed: 18096699]
25. Hoffmann C, et al. Caveolin limits membrane microdomain mobility and integrin-mediated uptake of fibronectin-binding pathogens. J Cell Sci. 2010; 123:4280–4291. [PubMed: 21098633]
26. Fra AM, Williamson E, Simons K, Parton RG. Detergent-insoluble glycolipid microdomains in lymphocytes in the absence of caveolae. J Biol Chem. 1994; 269:30745–30748. [PubMed: 7982998]
27. Tomassian T, et al. Caveolin-1 Orchestrates TCR Synaptic Polarity, Signal Specificity, and Function in CD8 T Cells. J Immunol. 2011; 187:2993–3002. [PubMed: 21849673]
28. Schönle A, et al. Caveolin-1 regulates TCR signal strength and regulatory T-cell differentiation into alloreactive T cells. Blood. 2016; 127:1930–1939. [PubMed: 26837700]
29. Medina FA, Williams TM, Sotgia F, Tanowitz HB, Lisanti MP. A novel role for caveolin-1 in B lymphocyte function and the development of thymus-independent immune responses. Cell Cycle. 2006; 5:1865–1871. [PubMed: 16929183]
30. Drab M, et al. Loss of caveolae, vascular dysfunction, and pulmonary defects in caveolin-1 gene-disrupted mice. Science. 2001; 293:2449–2452. [PubMed: 11498544]
31. Kenworthy AK, Petranova N, Edidin M. High-resolution FRET microscopy of cholera toxin B-subunit and GPI-anchored proteins in cell plasma membranes. Mol Biol Cell. 2000; 11:1645–1655. [PubMed: 10793141]
32. Schmitz R, Baumann G, Gram H. Catalytic Specificity of Phosphotyrosine Kinases Blk, Lyn, c-Src and Syk as Assessed by Phage Display. J Mol Biol. 1996; 260:664–677. [PubMed: 8709147]
33. Cao H, Courchesne WE, Mastick CC. A phosphotyrosine-dependent protein interaction screen reveals a role for phosphorylation of caveolin-1 on tyrosine 14: recruitment of C-terminal Src kinase. J Biol Chem. 2002; 277:8771–8774. [PubMed: 11805080]
34. Maity PC, et al. B cell antigen receptors of the IgM and IgD classes are clustered in different protein islands that are altered during B cell activation. Sci Signal. 2015; 8:ra93–ra93. [PubMed: 26373673]
35. Lee W-Y, Tolar P. Activation of the B cell receptor leads to increased membrane proximity of the Igα cytoplasmic domain. PLoS ONE. 2013; 8:e79148. [PubMed: 24244439]
36. Razani B, et al. Caveolin-1 null mice are viable but show evidence of hyperproliferative and vascular abnormalities. J Biol Chem. 2001; 276:38121–38138. [PubMed: 11457855]
37. Park DS, et al. Caveolin-1 Null (−/−) Mice Show Dramatic Reductions in Life Span. Biochemistry. 2003; 42:15124–15131. [PubMed: 14690422]
38. Gay D, Saunders T, Camper S, Weigert M. Receptor editing: an approach by autoreactive B cells to escape tolerance. J Exp Med. 1993; 177:999–1008. [PubMed: 8459227]
39. Pelanda R, et al. Receptor editing in a transgenic mouse model: site, efficiency, and role in B cell tolerance and antibody diversification. Immunity. 1997; 7:765–775. [PubMed: 9430222]
40. Treanor B, Depoil D, Bruckbauer A, Batista FD. Dynamic cortical actin remodeling by ERM proteins controls BCR microcluster organization and integrity. J Exp Med. 2011; 208:1055–1068. [PubMed: 21482698]
41. Vargas L, et al. Functional interaction of caveolin-1 with Bruton's tyrosine kinase and Bmx. J Biol Chem. 2002; 277:9351–9357. [PubMed: 11751885]
42. Jo A, et al. SHP-2 binds to caveolin-1 and regulates Src activity via competitive inhibition of CSK in response to H2O2 in astrocytes. PLoS ONE. 2014; 9:e91582. [PubMed: 24632723]
43. Radel C, Rizzo V. Integrin mechanotransduction stimulates caveolin-1 phosphorylation and recruitment of Csk to mediate actin reorganization. Am J Physiol Heart Circ Physiol. 2005; 288:H936–45. [PubMed: 15471980]
44. Gupta N, DeFranco AL. Lipid rafts and B cell signaling. Semin Cell Dev Biol. 2007; 18:616–626. [PubMed: 17719248]

45. Treanor B, Depoil D, Bruckbauer A, Batista FD. Dynamic cortical actin remodeling by ERM proteins controls BCR microcluster organization and integrity. J Exp Med. 2011; 208:1055–1068. [PubMed: 21482698]

46. Muriel O, et al. Phosphorylated filamin A regulates actin-linked caveolae dynamics. J Cell Sci. 2011; 124:2763–2776. [PubMed: 21807941]

47. Sohn HW, Tolar P, Pierce SK. Membrane heterogeneities in the formation of B cell receptor-Lyn kinase microclusters and the immune synapse. J Cell Biol. 2008; 182:367–379. [PubMed: 18644892]

48. Huck S, Corre RL, Youinou P, Zouali M. Expression of B Cell Receptor-Associated Signaling Molecules in Human Lupus. Autoimmunity. 2001; 33:213–224. [PubMed: 11683380]

49. Ng Y-S, Wardemann H, Chelnis J, Cunningham-Rundles C, Meffre E. Bruton's tyrosine kinase is essential for human B cell tolerance. J Exp Med. 2004; 200:927–934. [PubMed: 15466623]

50. Sproul TW, Malapati S, Kim J, Pierce SK. Cutting Edge: B Cell Antigen Receptor Signaling Occurs Outside Lipid Rafts in Immature B Cells. J Immunol. 2000; 165:6020–6023. [PubMed: 11086032]

51. Kim KJ, Kanellopoulos-Langevin C, Merwin RM, Sachs DH, Asofsky R. Establishment and characterization of BALB/c lymphoma lines with B cell properties. J Immunol. 1979; 122:549–554. [PubMed: 310843]

52. Hobeika E, et al. Testing gene function early in the B cell lineage in mb1-cre mice. Proc Natl Acad Sci. 2006; 103:13789–13794. [PubMed: 16940357]

53. Navarro-Lerida I, et al. A palmitoylation switch mechanism regulates Rac1 function and membrane organization. EMBO J. 2011; 31:534–551. [PubMed: 22157745]

54. Seppälä IJ, Mäkelä O. Adjuvant effect of bacterial LPS and/or alum precipitation in responses to polysaccharide and protein antigens. Immunology. 1984; 53:827–836. [PubMed: 6209209]

55. Fiala GJ, et al. Kidins220/ARMS binds to the B cell antigen receptor and regulates B cell development and activation. J Exp Med. 2015; 212:1693–1708. [PubMed: 26324445]

56. Belver L, de Yébenes VG, Ramiro AR. MicroRNAs Prevent the Generation of Autoreactive Antibodies. Immunity. 2010; 33:713–722. [PubMed: 21093320]

Europe PMC Funders Author Manuscripts

Europe PMC Funders Author Manuscripts

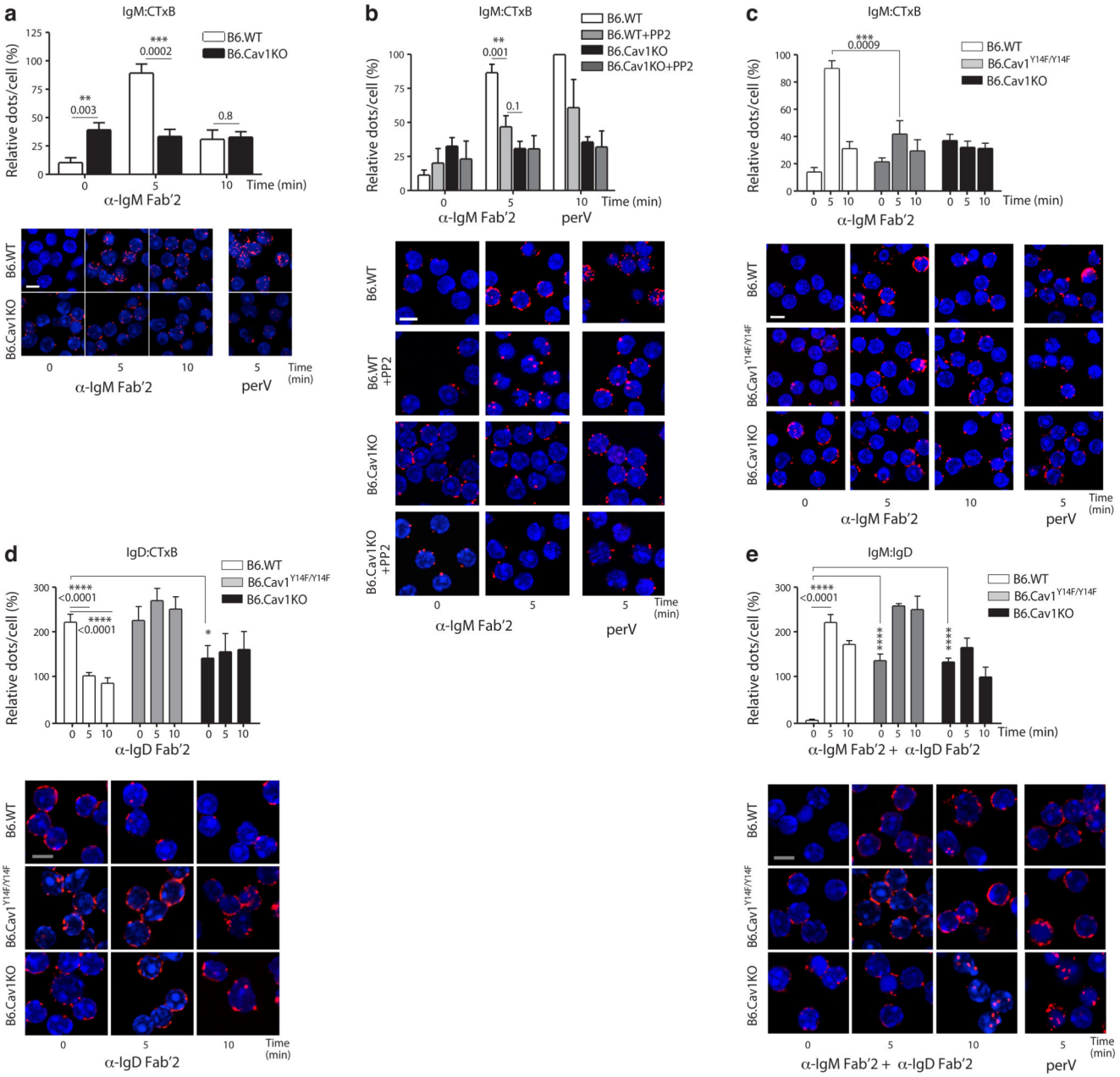

Figure 1. Cav1 regulates IgM- and IgD-BCR nanoclustering.

(**a**) Purified splenic B cells were stimulated with 10 μg/ml of anti-IgM Fab'2 for the indicated times or left unstimulated. PLA analyzes the proximity between the IgM-BCR and GM1-ganglioside. PLA signals (red dots per cell) were counted and normalized to the PLA signals of B6.WT cells stimulated for 5 min with 0.5 mM pervanadate (perV) for each individual experiment. Representative microscope images show DAPI stained nuclei (in blue) and PLA signals (in red). (**b**) Purified splenic B cells were pretreated with 10 μM PP2 or vehicle for 60 min before being stimulated and analyzed as in a. (**c**) Cells were stimulated and analyzed as in a. ANOVA P=0.004. (**d**) Purified splenic B cells were stimulated with 10 μg/ml of anti-IgD Fab'2 for the indicated times or left unstimulated. PLA analyzes the

proximity between the IgD-BCR and GM1-ganglioside. ANOVA P=0.05. (**e**) Purified splenic B cells were stimulated with 10 μg/ml of anti-IgM Fab‘2 and anti-IgD Fab‘2 for the indicated times. PLA analyzes the proximity between IgM-BCR and IgD-BCR. ANOVA P<0.0001.

In all panels, quantified data of at least three experiments were pooled and statistical analysis performed using unpaired Student’s t test when two conditions were compared. ANOVA test was used to compare B6.Cav1KO and B6.Cav1Y14F to B6.WT samples in unstimulated conditions followed by Dunnett's multiple comparisons. When significant, P values are indicated. Means ± SEM are shown. At least 300 cells were quantified per experimental condition and experiment. Size bar 5 μm.

Europe PMC Funders Author Manuscripts

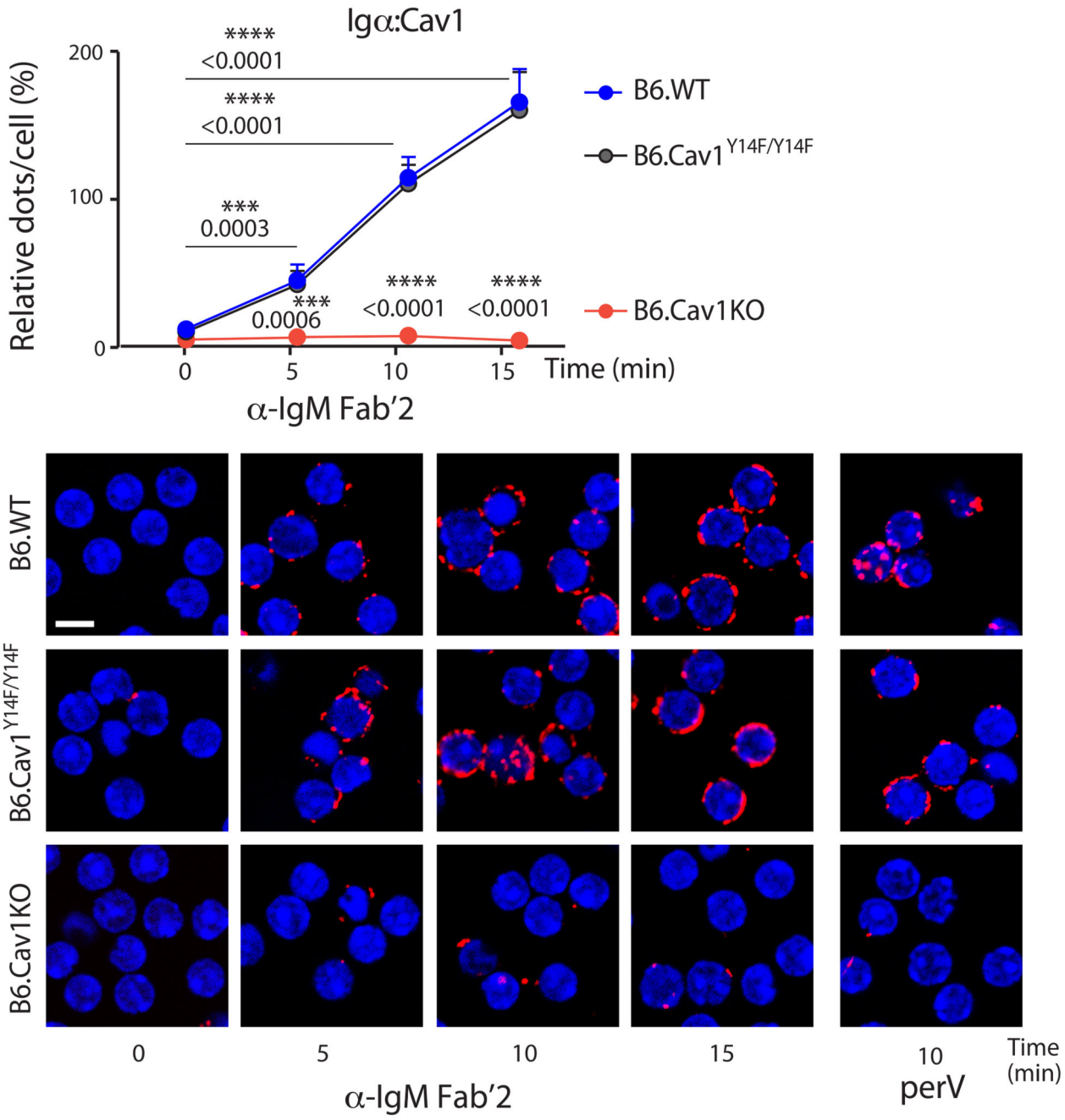

Figure 2. Cav1 and the BCR get in close proximity upon BCR stimulation.

Purified splenic B cells were stimulated with 10 μg/ml of anti-IgM Fab'2 for the indicated times or left unstimulated. Cells were fixed, permeabilized and *in situ* PLA analyzes the proximity between the Igα cytoplasmic tail and Cav1. PLA signals (red dots per cell) were counted and normalized to the PLA signals of perV-stimulated B6.WT cells for each individual experiment. Representative microscope images show DAPI stained nuclei (in blue) and PLA signals (in red). Five independent experiments were pooled and statistical analysis performed using Student's *t*-test. Means ± SEM are shown. P values between

resting and stimulated B6.WT cells, and between B6.WT and B6.CavKO samples are indicated. At least 300 cells were quantified per experimental condition and experiment. Size bar 5 μm.

Europe PMC Funders Author Manuscripts

Europe PMC Funders Author Manuscripts

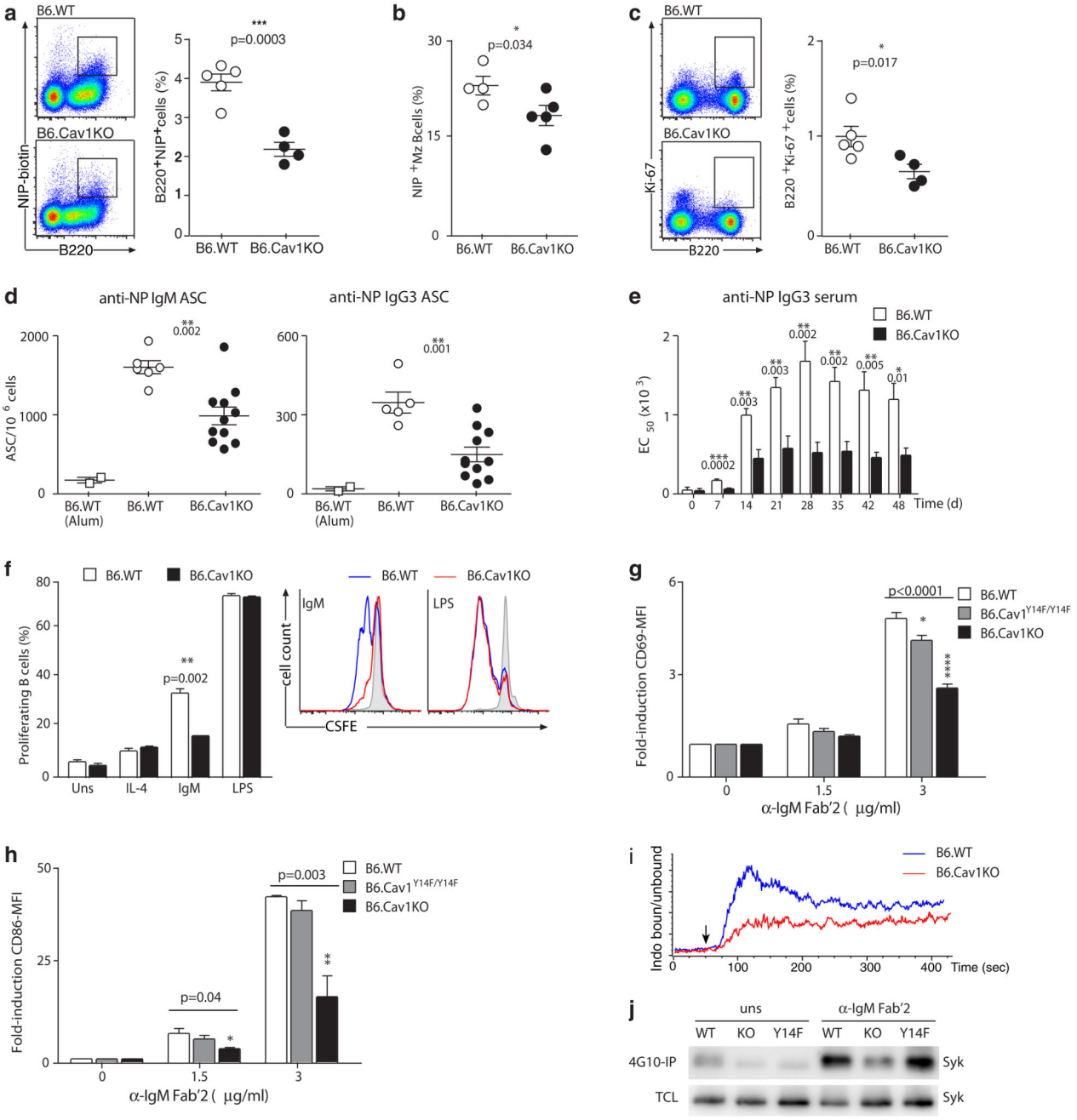

Figure 3. Absence of Cav1 reduces B cell responses in B6.CavKO mice.

(**a**) B6.WT and B6.CavKO mice were immunized with alum-precipitated NP-Ficoll. Splenocytes were analyzed for the frequency of NP-reactive B cells. Representative dot plots and the Mean ± SEM from 4-5 mice per group are shown. (**b**) NP-reactive Marginal zone (Mz) B cells and (**c**) the frequency of proliferating Ki-67^{+} B cells were analyzed. Representative dot plots and quantification plotted as in a are shown. (**d**) ELISPOT analysis of splenic NP-specific IgM-secreting cells (left) and NP-specific IgG3-secreting cells (right) 7 days after immunization with alum-precipitated NP-Ficoll. B6.WT mice injected only with

Alum served as a control. Data of two independent experiments were pooled, and the mean ± SEM from 6-11 mice per group is shown. (**e**) ELISA of NP-specific IgG3 from NP-Ficoll immunized mice. Serial dilutions of the serum were performed and the EC_{50} for each mouse calculated. (**f**) CSFE-labeled splenic B cells were stimulated with IL-4 (50 ng/ml) alone or in combination with 3 μg/ml anti-IgM Fab'2, 1 μg/ml LPS or were left untreated (grey shaded in the representative histogram). After 3 days, the proliferation-induced dilution of the CFSE dye was measured by flow cytometry. Data are representative of 2 independent experiments. (**g** and **h**) Purified splenic B cells were stimulated 18 hours and then analyzed for CD69 (**g**) and CD86 (**h**) expression by flow cytometry. Quantification shows pooled data from 2 independently performed experiments. ANOVA test was used to compare B6.Cav1KO and B6.Cav1Y14F to B6.WT samples; Dunnett's multiple comparisons P values are indicated on the top of the corresponding bar. (**i**) Calcium flux was measured by flow cytometry. Baseline was acquired for 50 sec, and then 8 μg/ml of α-IgM Fab'2 fragments were added (arrow, n=2). (**j**) Purified B cells were stimulated with 10 μg/ml anti-IgM Fab'2 for 5 min or left unstimulated. Cells were lysed, an aliquot of the total cellular lysate (TCL) kept and the rest of the lysate incubated with 4G10-coupled beads overnight. Proteins were then separated by SDS-PAGE and Syk detected by immunoblot (n=3). At least otherwise indicated, statistical analysis was performed using unpaired Student's *t*-test. Means ± SEM are shown. P values are indicated in each panel.

Europe PMC Funders Author Manuscripts

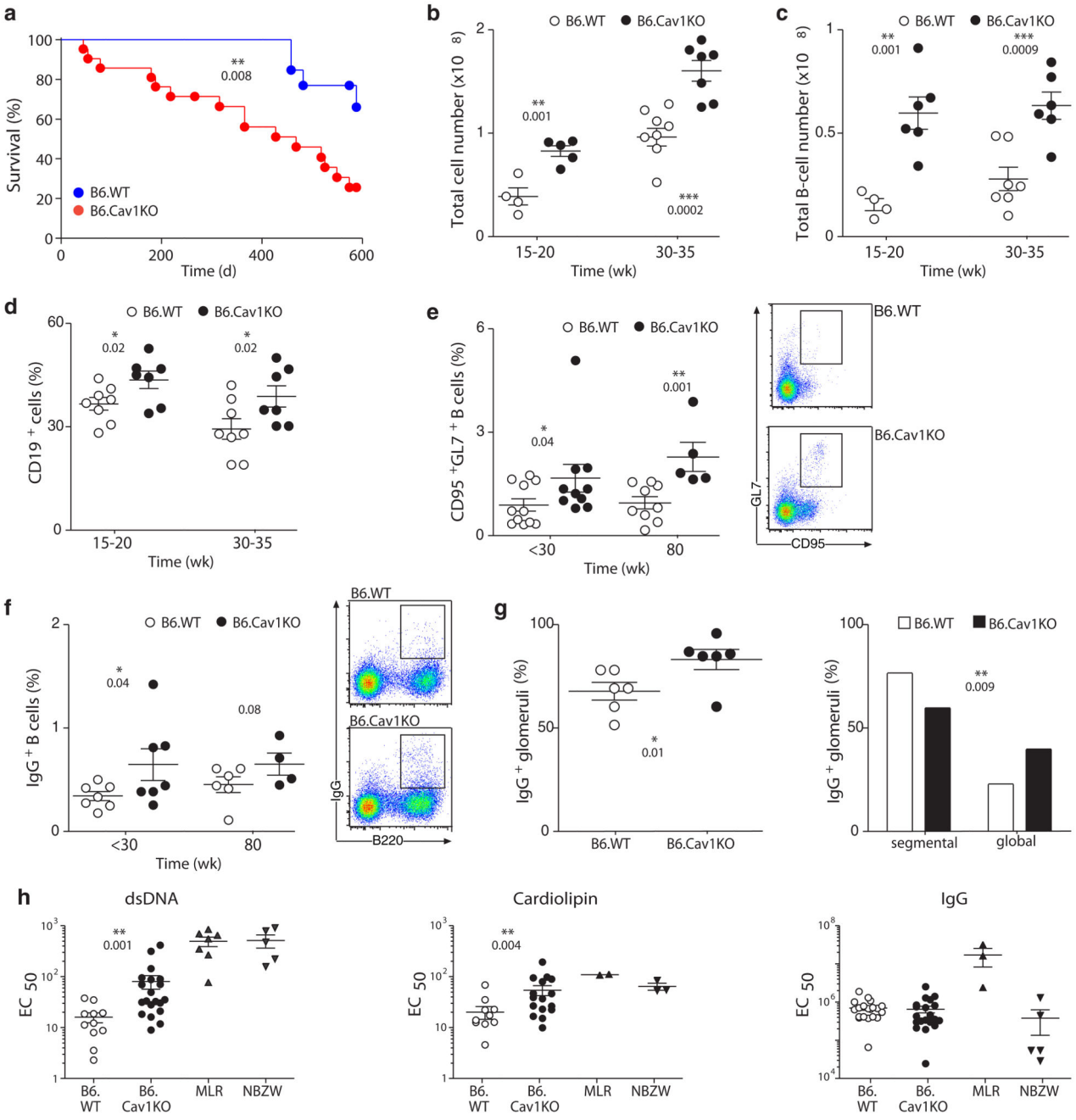

Figure 4. Increased B cell numbers, spontaneous GC formation, autoantibodies and reduced life span in B6.CavKO mice

(**a**) Survival curves of B6.WT and B6.CavKO mice. The Log-rank (Mantel-Cox) Test was applied and the P value indicated. (**b**) The total number of splenocytes in B6.WT and B6.CavKO was calculated in adult mice (15-20 weeks) and in aged mice (30-35 weeks). (**c**) Total B cell numbers and (**d**) the relative proportions of B cells in the spleen. (**e**) Proportion of splenic GC B cells of untreated adult mice (<30 weeks) and very old mice (80 weeks). Representative dot plots are provided. (**f**) Proportion of splenic class-switched IgG1^{+} B cells.

Representative dot plots are shown. (**g**) The kidneys of 80 weeks old mice were analyzed for the percent of glomeruli with IgG deposits (left). IgG^+ glomeruli were further analyzed for segmental (<50%) or global (>50%) distribution of IgG. Chi-squared contingency analysis was done. (**h**) The presence of anti-dsDNA (left), anti-cardiolipin (middle) and total IgG-antibodies (right) in the serum of old mice (50-80 weeks) was assayed by ELISA. Serial dilutions of the serum were performed and the EC_{50} for each mouse calculated. As positive control, serum from autoimmune MLR/lpr and NBZW mice were used. Normal data distribution was tested using Kolmogorov-Smirnov test. Statistical analysis was done using Mann Whitney test. Each dot represents an individual animal. Statistical analysis was performed using Student's *t*-test except in (h). Means ± SEM are shown. P values are indicated.

Europe PMC Funders Author Manuscripts

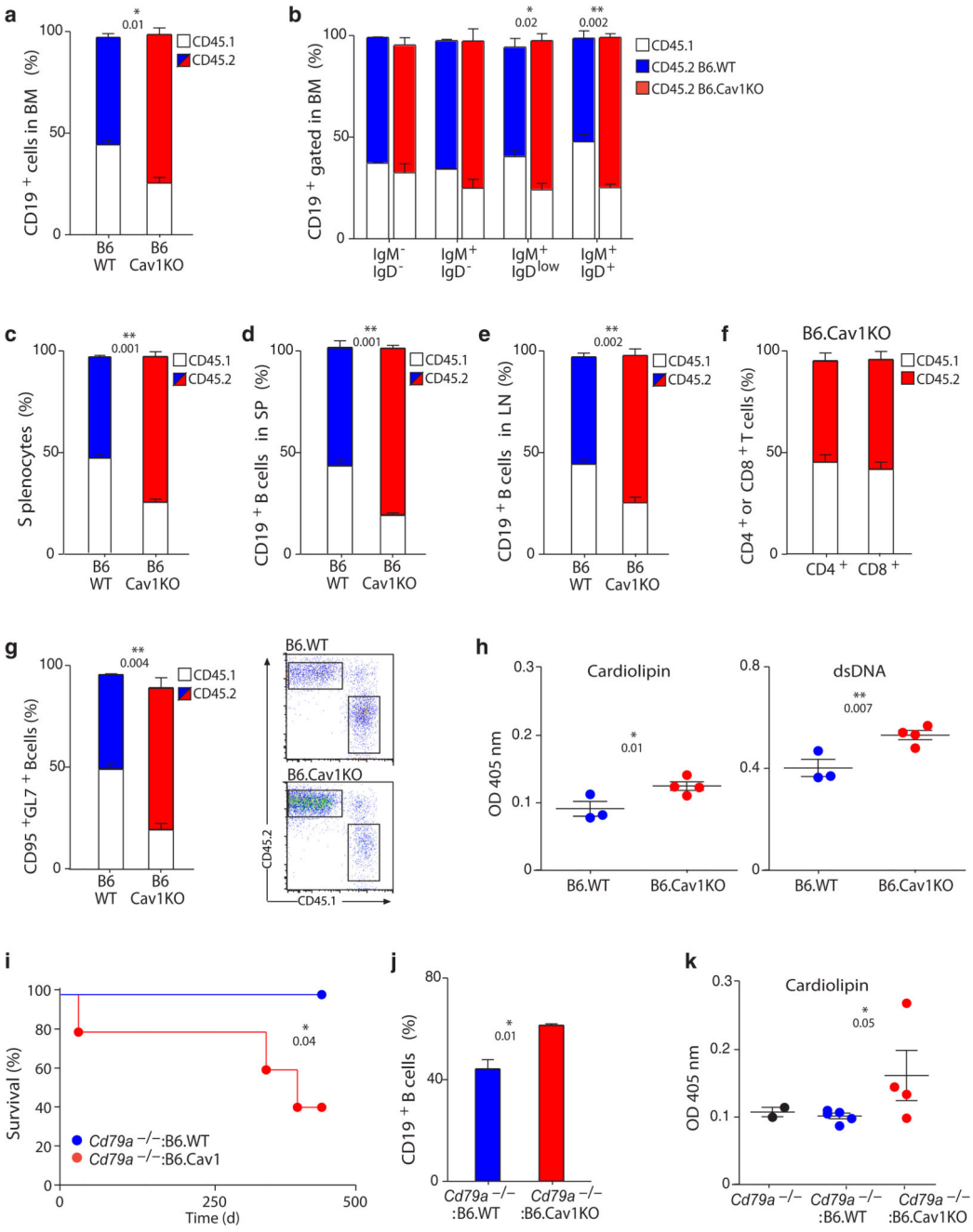

Figure 5. Cav1$^{-/-}$ B cells have a competitive advantage in bone marrow repopulation.

(**a-h**) B6.CD45.1 BM cells were mixed 1:1 with B6.WT or B6.CavKO BM cells and injected in sub-lethally irradiated Rag2$^{-/-}$γc$^{-/-}$ mice. Mice were analyzed 24 weeks after injection. (**a**) Percent of wild-type CD45.1^{+} (white) and CD45.2^{+} (blue for B6.WT and red for B6.CavKO) B cells in the BM (n=3-4). (**b**) Average chimerism of gated CD19^{+} B cells in the BM along B cell development (n=3-4). (**c**) Percent of CD45.1^{+} and CD45.2^{+} splenocytes (n=3-4). (**e** and **f**) Average chimerism on gated CD19^{+} B cells in the spleen (SP, **d**) and lymph nodes (LN, **e**). (**f**) Percent of CD45.1^{+} and CD45.2^{+} cells on gated CD4^{+} (left

column) or $CD8^+$ (right column) T cells in the B6.WT(CD45.1):B6.CavKO(CD45.2) chimeras (n=4). (**g**) Average chimerism on gated splenic GC B cells (n=3-4). Representative dot plots are shown. (**h**) Anti-cardiolipin (left) or anti-dsDNA (right) IgG in the serum of recipient mice assayed by ELISA (n=3-4). (**i-k**) B6.*Cd79a*$^{-/-}$ BM cells were mixed 1:1 with B6.WT or B6.CavKO BM cells and injected in sub-lethally irradiated Rag2$^{-/-}\gamma c^{-/-}$ mice. Mice were analyzed 63 weeks after injection. (**i**) Survival curves of the reconstituted mice. The Log-rank (Mantel-Cox) Test was applied and the P value indicated. (**j**) Percentage of splenic $CD19^+$ B cells of recipient mice (n=4). (**k**) Anti-cardiolipin IgG in the serum of recipient mice 45 weeks after transplantation assayed by ELISA (n=4). Serum from aged matched B6.*Cd79a*$^{-/-}$ mice was used as control. Each dot represents an individual animal. Statistical analysis was performed using Student's *t*-test. Means ± SEM are shown. P values are indicated.

Europe PMC Funders Author Manuscripts

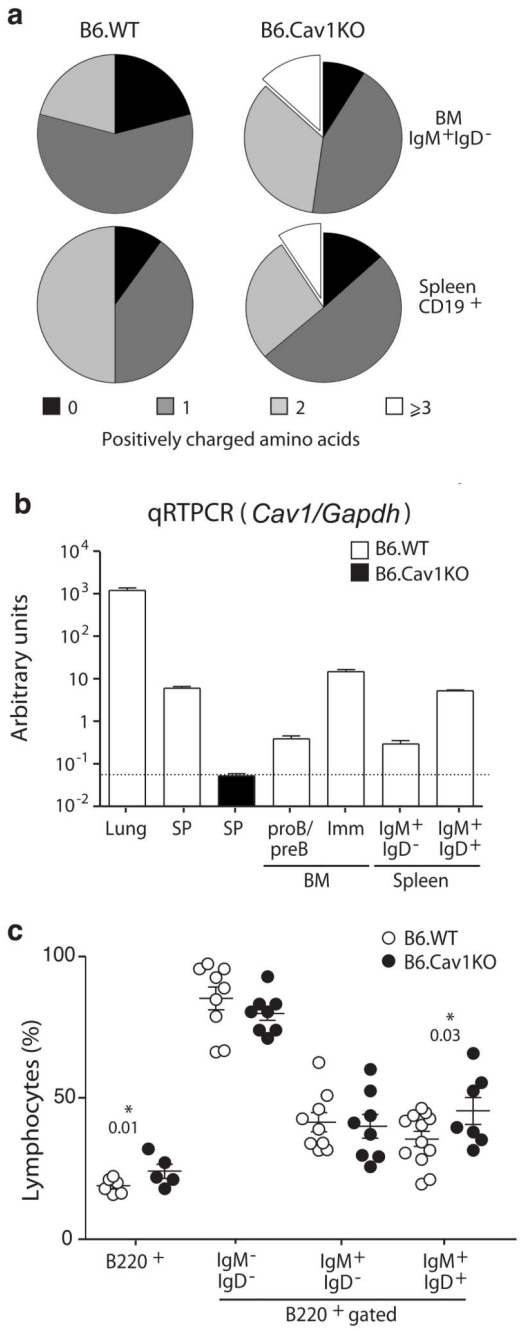

Figure 6. Cav1$^{-/-}$ B cells express a skewed IgH repertoire.

(**a**) The indicated B cell populations from BM and spleen were sorted, RNA extracted, retrotranscribed and PCR-amplified. PCR products were cloned, sequenced, and analyzed with the IgBlast software. A total of 128 sequences were analyzed. Results were obtained from two independent animals of each genotype (12 weeks old). Fischer's exact test p=0.0029 (**). (**b**) Quantitative PCR analysis of *Cav1* transcripts of single cell suspension of the indicated organs (lung, BM and SP, spleen) or sorted cell populations. Levels were normalized to *Gapdh* transcripts. Data from three independent RNA preparations were

pooled and are shown as Means ± SEM. (**c**) BM development was analyzed by flow cytometry. Each dot represents an individual animal (n=5-12, 12-20 weeks old). Statistical analysis was performed using paired Student's *t*-test. Means ± SEM are shown. Significant P values are indicated.

Europe PMC Funders Author Manuscripts

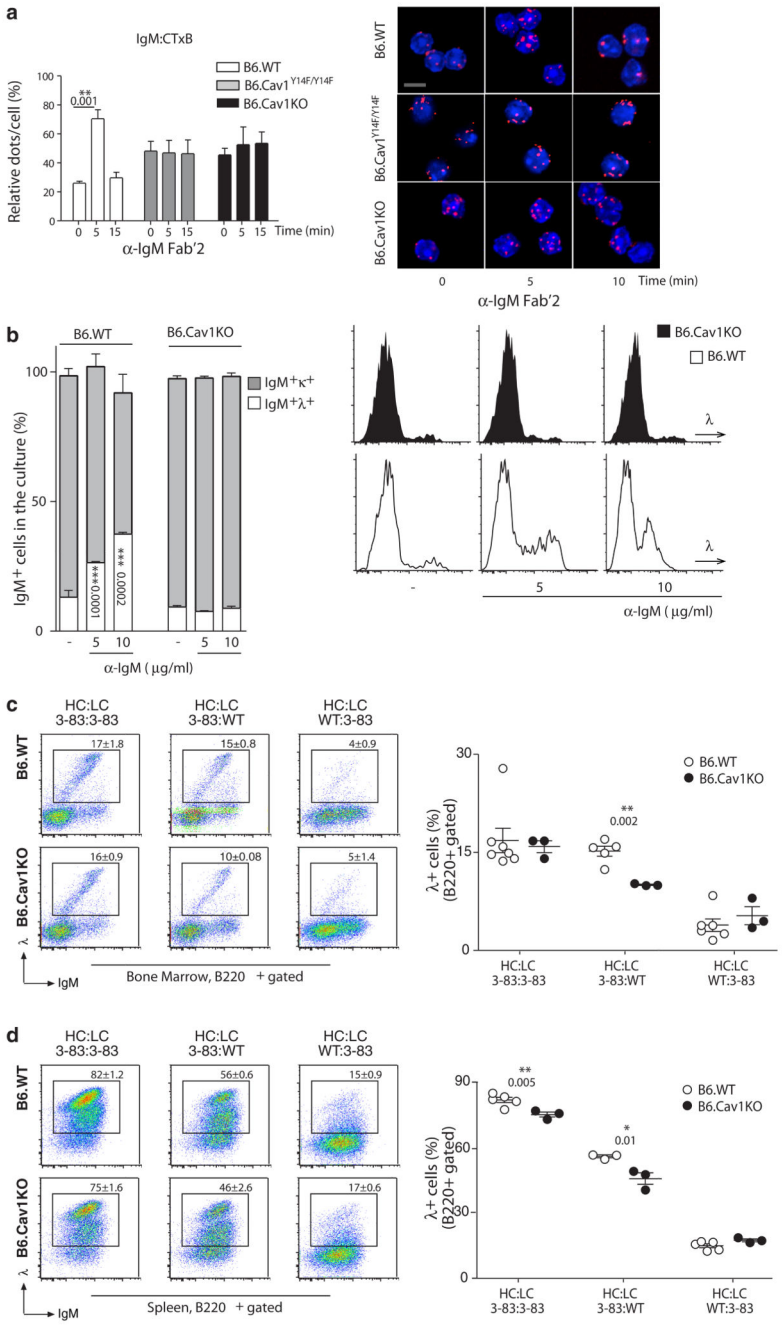

Figure 7. Defective receptor editing in B cells lacking Cav1 expression.

(**a**) Untouched immature B cells ($B220^{+}IgM^{+}IgD^{-}$) were purified. Cells rested for 3-6 hours in complete medium and stimulated and analyzed as described in Figure 1. Quantified data of 2-4 independent experiments were pooled. At least 100 cells were quantified per experimental condition and experiment. Size bar 5 μm. (**b**) BM cells were grown *ex vivo* for 6 days. The proportion of $IgM^{+}\lambda^{+}$ cells at day 6 of culture in the presence or absence of anti-IgM Fab'2 fragments is plotted as the Mean ± SEM. Representative histograms are shown. (**c** and **d**) B6.Cav1 mice were crossed with B6.3-83 mice, whose BCR, 3-83 heavy

Europe PMC Funders Author Manuscripts

chain (HC) and 3-83 κ light chain (LC), is autoreactive in the H-2b background (BL6). The expression of novel λLC^+ assayed by flow cytometry in the bone marrow (**c**) and spleen (**d**) indicates receptor editing. Each dot represents an individual animal (n=3-7). Statistical analysis was performed using Student's *t*-test. When significant, P values are indicated.

Europe PMC Funders Author Manuscripts